Rationally Designed Pooled CRISPRi-seq Uncovers a Novel Inhibitor of Bacterial Peptidyl-tRNA Hydrolase

A. S. M. Zisanur Rahman[1], Egor A. Syroegin[2], Lukas Timmerman[3], Julieta Novomisky Nechcoff[1], Archit Devarajan[1], Yury S. Polikanov[2], Silvia T. Cardona[1,4*]

[1]Department of Microbiology, University of Manitoba, Winnipeg, MB, Canada

[2]Department of Biological Sciences, University of Illinois at Chicago, Chicago, IL, USA

[3]Department of Computer Science, University of Manitoba, Winnipeg, MB, Canada

[4]Department of Medical Microbiology and Infectious Diseases, University of Manitoba, Winnipeg, Canada

*To whom correspondence should be addressed: silvia.cardona@umanitoba.ca

Abstract

Pooled knockdown libraries of essential genes are useful tools for elucidating the mechanisms of action of antibacterial compounds, a pivotal step in antibiotic discovery. However, achieving genomic coverage of antibacterial targets poses a challenge due to the uneven proliferation of knockdown mutants during pooled growth, leading to the unintended loss of important targets. To overcome this issue, we introduce CIMPLE (CRISPRi-mediated pooled library of essential genes), a rationally designed pooled knockdown library built in a model antibiotic-resistant bacteria, *Burkholderia cenocepacia*. By analysing growth parameters of clonal knockdown populations of an arrayed CRISPRi library, we predicted strain depletion levels during pooled growth and adjusted mutant relative abundance, achieving genomic coverage of antibacterial targets during antibiotic exposure. We demonstrate the utility of CIMPLE for chemogenetic profiling of known antibacterials and a previously discovered bacterial growth inhibitor of a new class. CRISPRi-Seq with CIMPLE, followed by biochemical validation, revealed that the novel compound targets the ribosome-associated quality control apparatus (RQC) by inhibiting the peptidyl-tRNA hydrolase (Pth). Overall, CIMPLE leverages the advantages of arrayed and pooled CRISPRi libraries to uncover unexplored targets for antibiotic action.

Keywords

Essential genes, CRISPRi, CRISPRi-Seq, Antibiotic mechanisms of action, Peptidyl-tRNA hydrolase, ribosome-associated quality control, RQC, Arrayed library, Pooled library

Summary

Bacterial mutant libraries in which antibiotic targets are downregulated are useful tools to functionally characterize novel antimicrobials. These libraries are used for chemogenetic profiling as target-compound interactions can be inferred by differential fitness of mutants during pooled growth. Mutants that are functionally related to the antimicrobial mode of action are usually depleted from the pool upon exposure to the drug. Although powerful, this method can fail when the unequal proliferation of mutant strains before exposure causes mutants to drop out of the library

pool. To address this issue, we constructed an arrayed essential gene mutant library (EGML) in the antibiotic-resistant bacterium *Burkholderia cenocepacia* using CRISPR interference (CRISPRi) and analyzed the growth parameters of individual mutant strains. We then modelled depletion levels during pooled growth and used the model to rationally design an optimized CRISPR interference-mediated pooled library of essential genes (CIMPLE). By adjusting the initial inoculum of the knockdown mutants, we achieved coverage of the bacterial essential genome with mutant sensitization. We exposed CIMPLE to a recently discovered antimicrobial of a novel class and discovered it inhibits the peptidyl-tRNA hydrolase, an important component of ribosome recycling during translation. In summary, we demonstrate the utility of CIMPLE and CRISPRi-seq to uncover the mechanism of action of novel antimicrobial compounds.

Author contributions

ASMZR - performed the majority of the experiments and wrote the manuscript

EAS- synthesized peptidyl-tRNA, purified Pth_{BC}, and performed Pth_{BC} activity assay

LT- created the Python script to design sgRNAs

JNN - contributed to the library preparation for CRISPRi-Seq and edited the manuscript

AD- contributed to the hypersensitivity assay of the depleted mutants from pilot CRISPRi-Seq

YSP – supervised the work, acquired funding, and reviewed the manuscript

STC- conceived the idea, supervised the work, provided financial support, and edited the final version of the manuscript.

Introduction

Antibiotic-resistant infections challenge public health and underscore the need for antibiotics of novel classes. In response, targeting the products of essential genes, which govern bacterial growth and viability, stands as one of the pivotal arms of early antibiotic drug discovery[1]. Essential gene mutant libraries (EGMLs) are useful tools to determine the mode of action of novel antimicrobials[2,3]. By downregulating an essential gene product, particular EGML strains are sensitized to compounds targeting that product or a functionally related function. Consequently, the collective growth response of an EGML exposed to an antimicrobial can generate a chemical-genetic profile of the drug, thus providing an initial characterization of its mode of action (MOA)[4,5].

CRISPR interference (CRISPRi)[6] is an ideal tool for creating EGMLs as it allows inducible repression of essential gene expression in bacteria[7]. CRISPRi utilizes a catalytically dead Cas9 (dCas9) and a single guide RNA (sgRNA)[6]. The dCas9 and sgRNA form a DNA-recognizing complex that binds to the target DNA and sterically blocks transcription. Recognition of the target gene requires a short sequence called protospacer adjacent motif (PAM)[8–10]. This PAM requirement constrains targeting and affects knockdown efficiency and target flexibility. CRISPRi can be applied to high throughput levels to create tunable[6,7] and reversible[11] CRISPRi mutant libraries. Several pooled[12–19] and arrayed[7,20–22] CRISPRi-based mutant libraries have been developed to facilitate the study of bacterial essential pathways[12,22–25], identification of antibiotic susceptibility determinants[18,20,26–30] and novel antimicrobial MOA[7]. Pooled libraries, which typically involve disrupting essential genes *en masse*, offer streamlined construction. However, these libraries are complex in number and risk disproportionate representation or even absence of essential gene mutants due to uneven growth. In contrast, arrayed libraries are smaller and have individual mutant strains representing the whole essential genome. However, profiling antimicrobials with arrayed CRISPRi libraries is costly as each mutant must be grown individually and exposed to the antimicrobials under investigation.

In this study, we describe the construction and use of CIMPLE (optimized CRISPRi-mediated pooled library of essential genes), which combines the advantages of arrayed and pooled CRISPRi libraries. Developed in a multiple antibiotic-resistant bacterium, *Burkholderia cenocepacia* K56-2[31], CIMPLE is a pooled CRISPRi library created from an ordered CRISPRi

collection. By quantifying the growth parameters of clonal mutant populations and modelling mutant depletion during pooled growth, we rationally manipulated the initial relative abundance of the mutants in the pool to achieve genomic coverage of sensitized mutants. The CIMPLE platform, followed by CRISPRi-Seq, generated the chemical genetic profile of a novel growth inhibitor and signalled ribosome recycling as the essential function affected. Further biochemical characterization identified the peptidyl-tRNA hydrolase as the target of the novel compound. In summary, CIMPLE leverages the benefits of arrayed and pooled mutant libraries and demonstrates success in the characterization of a novel antimicrobial mode of action.

Results

Construction and characterization of an arrayed essential gene knockdown mutant library (EGML) with CRISPRi technology

To construct the EGML in *B. cenocepacia* K56-2*,* we used our previously developed CRISPRi toolkit for *Burkholderia*[32], in which a chromosomal copy of the *Streptococcus pyogenes* dCas9 ($dCas9_{Spy}$) is expressed from a rhamnose-inducible promoter and sgRNAs are constitutively expressed from a plasmid (**Fig. 1A**). We confirmed that $dCas9_{Spy}$ PAM preference allows more targetable regions in the *B. cenocepacia* K56-2 genome compared to other orthologous dCas9 proteins (**Supplementary Fig. 1**; **Supplementary Table 1**; **Supplementary Note 1**). To develop the arrayed CRISPRi library, we targeted the K56-2 essential genome comprising 535 genes[33,34]. Based on the predicted operons in the closely related *B. cenocepacia* J2315 [35,36] (**Supplementary Table 2)** and the polar effect of CRISPRi[6,7], the number of target sites was reduced to ~450.

Gene silencing with CRISPRi is more efficient when transcription initiation is blocked by targeting the promoter region in the non-template strand[37,38]. As the transcription start sites for most *B. cenocepacia* essential operons are unknown, we evaluated whether sgRNAs could be designed based on the proximity to the translation start sites. Fifteen essential genes from different Cluster of Orthologous Genes (COGs) categories were targeted with sgRNAs designed at different distances from their translation start sites (**Supplementary Fig. 2A** and **Supplementary Table 3**). These sgRNAs were cloned into the sgRNA expressing vector, pgRNA, and introduced into *B. cenocepacia* K56-2::*dCas9*[32] via tri-parental mating. We observed defective growth phenotypes for all targeted genes (**Supplementary Fig. 2B**), in agreement with recent findings[6,14,32]. To design

sgRNA targeting all essential genes, we developed a custom sgRNA design pipeline **(Supplementary Fig. 3).** While computational tools for sgRNA design exist[39–46], they primarily cater to eukaryotic genomes and are not optimized for GC-rich organisms like *Burkholderia*. By combining the insights from our pilot study and published protocols[6,7,17,37,38], we designed 615 sgRNAs targeting the *B. cenocepacia* K56-2 essential genome[33,34] **(Supplementary Fig. 3; Supplementary Table 4**).

To test the efficiency of sgRNAs and evaluate the effect of CRISPRi-based silencing of the essential genes, we used saturating inducing conditions (1% rhamnose) as previously determined[32]. Mutants were grown clonally in microtiter plate format, and their growth phenotype was evaluated from the growth curves (**Supplementary Fig. 4A)** by calculating the maximum growth rate (μ_{max}) and apparent lag time (**Fig. 1B, C**). In non-inducing conditions, mutants and control exhibited similar growth parameters (median μ_{max} of 0.7 h^{-1} and 0.73 h^{-1}, and apparent lag time of 5.1 h and 5.2 h, respectively (**Fig. 1D**, **1E** -rhamnose). Upon induction of the CRISPRi system, mutants showed a deviation towards a lower μ_{max} and a more extensive apparent lag time (**Fig. 1D, 1E** +rhamnose). We arbitrarily designated mutants with a growth defective phenotype when they observed a 15% reduction in μ_{max} or a 15% longer apparent lag time in inducing conditions compared to the pgRNA-nontarget control. We obtained mutants with an observable growth defect in 92% of the essential gene targets.

To determine whether general essential functions can explain the observed variation in growth phenotypes, we sorted the mutants based on the COG categories and μ_{max} in the presence of rhamnose. We observed the slowest μ_{max} of the CRISPRi knockdown mutants targeting translation processes (COG J and O), membrane biogenesis (COG M) and DNA replication and repair (COG L) compared to the pgRNA-nontarget control ($p < 1\times10^{-5}$, t-test; **Supplementary Fig. 4B**). Eighty percent of the knockdown mutants had at least 15% longer apparent lag times compared to the pgRNA-nontarget control (**Fig. 1C and E**). Translation and cell wall-related mutants had the longest apparent lag time (**Supplementary Fig. 4B**), and some of the mutants never reached the exponential phase (**Supplementary Fig. 4A**). Together, the EGML growth phenotypes were very diverse, highlighting the differing essential functions under CRISPRi control. This diversity poses a challenge to chemogenetic profiling as sensitizing conditions (knockdown induction) may vary across the library [47,48].

Mutant depletion during pooled growth is explained by the combination of clonal μ_{max} and lag time

Two prerequisites are optimal for high throughput chemical-genetic profiling of novel antimicrobials using pooled essential gene libraries: i) individual knockdown depletion during pooled growth should be accurately detected; ii) the library must contain sensitized mutants representing the essential genome. Using sgRNA coding sequences as DNA barcodes for Illumina sequencing, we detected individual mutant depletion from artificially depleted mutant pools. We obtained strong correlation between biological replicates of CRISPRi-Seq with small (50) and large (150) mutant pools confirming the method's ability to detect changes in relative abundance accurately (**Supplementary Fig. 5**) and demonstrating its reliability (**Supplementary Fig. 6**). To find out whether the pooled EGML represented the *B. cenocepacia* K56-2 essential genome, the EGML mutants were equally arranged in a pooled inoculum (1X pool), allowed to grow at different rhamnose concentrations (**Supplementary Fig. 7)** and their relative abundance determined by CRISPRi-Seq. Non-inducing conditions (likely causing basal levels of dCas9 expression) were sufficient for reducing fitness in most of the mutants during pooled growth as approximately 77% of the mutants exhibited depletion above 25% (**Supplementary Fig. 8A**). In our experience, knockdown mutants partially depleted in essential gene products are specifically sensitized to their cognate growth inhibitors when their clonal growth is reduced between 30 and 60% with respect to the wild type [47,48]. In addition, a stronger growth reduction tends to cause general sensitivity to many stressful conditions. Because competitive growth enhances knockdown mutant sensitivity[47,] we established that sensitization during pooled growth could be achieved at less than 50% depletion levels. However, even in the mildest conditions, the pooled EGML contained 'mutants representing 120 essential targets that were depleted by more than 50%, probably reducing genomic coverage and increasing the chance of unspecific, non-informative response when exposed to antimicrobial compounds.

To construct a pooled EGML library with representation of the essential genome in sensitized conditions, we reasoned that if we could predict the depletion levels of specific mutants during pooled growth, we should be able to adjust the relative abundance of the mutants' inocula to balance growth and sensitization levels. We observed that neither apparent lag time nor μ_{max} of individual mutants were predictors of depletion levels during pooled growth (**Fig. 2A** and **B**).

Similarly, end-point maximum growth inhibition did not correlate with depletion during pooled growth (**Fig. 2C**). Because the growth rate of the knockdown mutants (μ_{max}) inversely correlated with the lag time (**Fig. 2D**), we reasoned that a combination of the individual growth parameters and mutant fitness due to competition would impact mutant depletion levels during pooled growth. We then used multivariate polynomial regression to model the relationship between the clonal features ($\mu_{max(+Rha)}$ and apparent lag time) and depletion levels during pooled growth (**Supplementary Note 2)**. Multivariate polynomial regression extends polynomial regression to multiple independent variables, capturing complex non-linear relationships through polynomial functions. The fitted model predicted depletion scores based on the relationship between the clonal features. We observed a strong correlation between the experimentally observed and predicted mutant depletion (**Fig. 2E**). Together, our analysis demonstrates that depletion levels during pooled growth can be predicted by combining the growth parameters of CRISPRi mutant clonal growth.

Rational design and construction of CIMPLE

The predicted depletion of CRISPRi mutants during pooled growth indicated that a pooled EGML would lack a complete representation of the *B. cenocepacia* K56-2 essential genome due to particular mutant dropouts (**Fig 2E**). We reasoned that manipulating the relative abundance of the CRISPRi mutants inocula could change the competition dynamics, increasing the number of sensitized mutants to achieve coverage of the essential genome in the final pool (**Fig. 3A**). In this scenario, mutants predicted to be depleted at different degrees ('sick and highly sick mutants') could be inoculated at different proportions (spiked pool) into distinct pools. Therefore, mutants expected to be depleted more than 75% (highly sick) in the equal EGML (1X pool) were inoculated at ratios of 5X, 10X, or 20X. Mutants with 60-75% depletion ('sick') were inoculated at ratios of 3X, 5X, or 10X, while mutants with 50-60% depletion ('sick') were inoculated at ratios of 2X, 3X, or 5X (**Supplementary Table 6**) resulting in three differentially-inoculated pools: 5X3X2X, 10X5X3X and 20X10X5X pools. We observed undesired mutant overrepresentation after growth from the 10X5X3X and 20X10X5X pools (**Supplementary Fig. 8B-C).** On the other hand, the 5X3X2X-inoculated pool demonstrated the highest proportion of sensitized mutants as most (~90 %) of the mutants were depleted less than 50% (**Fig. 3B**). While 67 mutants became highly abundant (enriched) in the 5X3X2X pool (compared to 57 in the equal EGML), pooled growth from the 5X3X2X-inoculated pool provided ~90% coverage of the *B. cenocepacia* K56-2 essential

genome in one single sensitizing condition (non-inducing) (**Supplementary Fig. 8D**). In contrast to the previous approaches with handling individual mutants[7] or multiple pools[3], our approach allowed us to essential gene coverage in one single condition, which can streamline and increase the throughput of chemogenetic profiling experiments.

To investigate the possible link between fitness during pooled growth and essential functions, we weighed the contribution of different parameters by a principal component analysis (PCA) and compared the obtained cluster of mutants with their COG categories. To that end, we used a Kernel PCA[49] combined with K-means clustering[50] and clustered the mutants based on μ_{max}, apparent lag time, mutants' pooled fitness and fold inoculum level in the 5X3X2X-inoculated pool. We clustered the mutants into three clusters based on K-means clustering and projected the mutants in two-dimensional PCA space (**Fig. 3C**). Mutants that were inoculated at 1X proportions comprised 98% of the mutants grouped in cluster 2, which was specifically enriched in the COG category DNA replication and repair (L) (**Fig. 3D**). On the other hand, mutants inoculated at the 5X proportion constituted 91% of cluster 3, which was enriched in translation (J), nucleotide metabolism and transport (F) and transcription (K). In contrast, cluster 1 was more diverse as only 50% of the mutants belonged to the group of mutants inoculated 2X and 3X (**Fig. 3D**). This cluster was also functionally diverse, containing the COG categories coenzyme metabolism (H), translation (J) and DNA replication and repair (L).

Overall, functional diversity of essential functions partially explained differential fitness during competitive growth. However, the prediction of depletion levels from clonal mutant growth guided a rationally designed pooled inoculum that changed the competition dynamics during pooled growth, increasing genomic coverage of essential genes and expected levels of sensitization. This approach enabled the creation of an optimized CRISPR interference-mediated pooled library of essential genes (CIMPLE) in *B. cenocepacia* K56-2.

CIMPLE followed by CRISPRi-Seq, captures drug-target interactions and the targets of known antimicrobials

CIMPLE should allow essential genome coverage to report antibiotic mechanism of action (MOA). For instance, the *dcw* operon (containing *ftsZ*) and *gyrB* were not detected in the 1X pool (100% depleted); however, by changing the corresponding mutants' relative abundance in the

5X3X2X inoculum, the *dcw* operon and *gyrB* genes were represented in CIMPLE (**Supplementary Fig. 9**). To confirm that CIMPLE can detect the depletion of specific mutants when treated with their cognate antibiotics and determine their MOA, we exposed it to a subinhibitory concentration (IC_{30}) of antibiotics from different classes with known cellular targets (**Fig. 4A** and **Supplementary Table 6**). We measured the relative abundance of the CRISPRi mutants from the pool in each treated condition and compared that to the DMSO control. The normalized relative abundance was highly correlated between the independent biological replicates (**Supplementary Fig. 10**). We focused on the significant chemogenetic interactions between compounds and essential gene mutants (**Fig. 4B-E**). When we exposed CIMPLE to C109, a benzothiadiazole derivative that targets FtsZ[48], we observed a significant depletion of the CRISPRi mutant targeting *dcw* cluster, which contains *ftsZ* (*dcw* cluster; BCAL3457 to BCAL3471; **Fig. 4B**). The *dcw* is an essential operon that maintains the cell division and cell wall synthesis in a regulated manner, starting with FtsA and FtsZ[51]. While we observed seven significantly depleted hits in the absence of rhamnose (including the specific target *dcw* cluster), the number of hits was higher in the presence of rhamnose (0.1%) which still included the CRISPRi mutants targeting the *dcw* operon (**Fig. 4C**). Likewise, both *gyrA* and *gyrB* targeting CRISPRi mutants were significantly depleted in the presence of novobiocin (**Fig. 4D-E**). Novobiocin is an aminocoumarin antibiotic that binds to the ATP binding site of GyrB (which acts by forming a complex with GyrA) and inhibits enzymatic activity by impeding ATP hydrolysis[52]. Novobiocin also caused significant depletion of DNA polymerase III subunit β (*dnaN*; BCAL0422), transcription termination factor Rho (*rho*; BCAL1901), holliday junction resolvase (*ruvC*; BCAL3337), a hypothetical protein (BCAL1364), and UDP-3-O-[3-hydroxymyristoyl] N-acetylglucosamine deacetylase (*lpxC*; BCAL3455). LpxC catalyzes the deacetylation of UDP-3-O-acyl-N-acetylglucosamine, which is a crucial step in the synthesis of lipid A. As a lipopolysaccharide (LPS) component, lipid A plays a critical role in the structural integrity of the outer membrane. While novobiocin and its analogs have been shown to affect the Lpt pathway and potentiate the activity of polymyxin[53], no direct interaction has been reported. Overall, we found that non-inducing conditions (0% rhamnose) were sufficient to capture an antibiotic susceptibility profile and to identify the specific cellular target.

CRISPRi-Seq identified peptidyl-tRNA hydrolase (Pth) as the direct target of PHAR(A)

We previously employed a deep learning model to predict bacterial growth inhibition in a natural product library containing over 224,000 compounds[54]. Our approach led to the identification of STL529920 (renamed to PHAR(A) herein), a growth inhibitory compound with a novel chemical scaffold[54]. PHAR(A) exhibited broad growth inhibitory activity against *B. cenocepacia* K56-2 and the ESKAPE pathogens[54] by an unknown mechanism. To elucidate PHAR(A) mechanism of action, we exposed CIMPLE to 50µM of PHAR(A) in non-inducing conditions and with 0.1% rhamnose. In the absence of rhamnose, CIMPLE exposure to PHAR(A) followed by CRISPRi-Seq revealed significant depletion of a CRISPRi mutant targeting the peptidyl-tRNA hydrolase (Pth; BCAL0798) (**Fig. 5A**). In the presence of 0.1% rhamnose, additional knockdown mutants of genes related to translation were significantly depleted from the pool including a hypothetical protein (WQ46_RS24220), 30S ribosomal protein S1 (*rpsA*; BCAL2950), amino-peptidase P (BCAL3332), tRNA-specific 2-thiouridylase MnmA (*mnmA*; BCAL3329) and WaaA (*waaA*; BCAL3110) (**Fig. 5B)**. CIMPLE response suggested that PHAR(A) interferes with the translation machinery, possibly directly inhibiting the Pth activity. Pth cleaves the ester bond between the tRNA and the peptide, releasing the tRNA for reuse in translation and the truncated peptide for degradation (**Fig. 5C**)[55]. Pth is highly conserved across bacterial species. The absence of Pth disrupts tRNA recycling in the cell during translation, leading to compromised translation initiation and reduced protein synthesis due to the depletion of specific tRNA and, subsequently, cell death[55,56]. The essential activity of the bacterial Pth makes it a high-value drug target.

To confirm the chemogenetic interactions evidenced by CRISPRi-Seq, the CRISPRi mutants that were significantly depleted in the presence of PHAR(A) were grown in sensitizing conditions (rhamnose concentration to inhibit growth in 30%, $RhaIC_{30}$) (**Supplementary Table 7**). The sensitized mutants were exposed to a PHAR(A) concentration gradient. The Pth knockdown mutant was the most sensitive compared to pgRNA-nontarget and *B. cenocepacia* K56-2 WT in the presence of PHAR(A) (**Fig. 5D)**, resembling CIMPLE profiling of PHAR(A). Albeit at a lower level, the other translation-related knockdown mutants (RpsA, MnmA, Aminopeptidase P, VirB1) were also sensitive in the presence of PHAR(A), reverberating the chemogenetic profile obtained by CRISPRi-Seq. To investigate if Pth is the target of PHAR(A), we purified *B. cenocepacia* K56-2 Pth (Pth_{BC}). We observed a dose-dependent inhibition of the recombinant *B. cenocepacia* K56-2 Pth activity by PHAR(A) starting from 15µM (PHAR(A) IC_{50}

= 34.2μM; (**Fig. 5E-F**)), but not by PHAR(A) analogs that did not have any growth inhibitory activity[54] (**Supplementary Fig. 11**). These results indicate that PHAR(A) is a specific inhibitor of the bacterial Pth and highlight the utility of CIMPLE to identify both direct and indirect drug-target interactions involved in the mechanism of action of novel bioactive compounds. To our knowledge, PHAR(A) is the first compound that targets and inhibits Pth enzymatic activity.

Discussion

Essential gene mutant libraries are useful tools for genetic interaction mapping to identify the mode of action of novel antibiotic drugs. Here, we have constructed a comprehensive, arrayed essential gene knockdown mutant library (EGML) targeting each of the identified *B. cenocepacia* K56-2 essential genes. Considering the mutants' growth when grown clonally and in a competitive pooled growth environment, we created an optimized CRISPRi-mediated pooled library of essential genes (CIMPLE) by predicting pooled depletion levels from clonal growth parameters and changing the relative abundance of the mutants in the pooled inoculum. We demonstrated the utility of CIMPLE in identifying the mechanism of action of known and novel bioactive compounds.

We started with the creation of an arrayed CRISPRi-based essential gene knockdown mutant library because they offer precise control over individual gene perturbations. A portion of the mutants did not show growth defect in the clonal growth environment in the presence of rhamnose (**Supplementary Fig. 4A**; **Fig. 2A-B**), possibly due to weak target gene repression of the proteins that have higher turnover rate or are required at a lower copy number for the essential function. However, we observed depletion of those mutants during pooled growth (**Fig. 2A-B**, **Supplementary Fig. 9A**), indicating that the competitive pooled growth can compensate for the frail target gene silencing to uncover the mutant phenotype. Although no clear linear correlation was observed between the pooled depletion and the apparent lag time or clonal growth rate when examined individually (**Fig. 2A-B**), our random forest-based approach enabled us to discern the interplay between the mutants' depletion during pooled growth and their clonal growth characteristics. This analysis unveiled that the pooled depletion is a function of both the clonal features (**Fig. 2E**).

We clustered the mutants with similar sensitization profiles to the depletion of the essential gene product by combining Kernel PCA with K-means clustering approach (**Fig. 3C**). Principal

component analysis (PCA) emphasizes the principal feature that contributes to the majority of variance within the query dataset. Like PCA, Kernel PCA effectively reduces dimensionality but excels in capturing non-linear relationships in the data[49]. We observed the enrichment of certain COG groups in different clusters (**Fig. 3D**), highlighting the variable effect of the depletion of these target proteins on the mutant growth within the COG.

CIMPLE was instrumental in representing the highly sick mutants (in the pool) that would have otherwise been missed in the 1X library. For example, the *dcw* operon (containing *ftsZ*), *gyrB*, and *dnaN* were absent in the 1X pool (100% depleted) (**Supplementary Fig. 9A**). FtsZ (part of the dcw cluster) is targeted by C109, GyrB is targeted by Novobiocin, and DnaN also plays a role in novobiocin-mediated sensitivity. By artificially altering their initial relative abundance in the CIMPLE library, we ensured their inclusion, allowing us to capture and reaffirm the mechanisms of action (MOA) of C109 and novobiocin (**Supplementary Fig. 9B**).

Leveraging CIMPLE, we identified the known drug-target interactions while uncovering novel mediators of novobiocin sensitivity. Our study identified the involvement of DnaN, Rho, LpxC and BCAL1364 as potential novel mediators of novobiocin sensitivity. DnaN, the β subunit of DNA polymerase III, plays a pivotal role in DNA replication, while Rho is an essential RNA helicase involved in transcription termination. The potential interaction between novobiocin and these critical cellular components suggests a nuanced mechanism underlying the antibiotic's efficacy. Inhibition of DnaN by novobiocin may disrupt DNA replication, leading to bacterial growth inhibition or cell death. Similarly, interference with Rho function could impede transcriptional regulation, affecting gene expression patterns crucial for bacterial survival. LpxC contributes to the biosynthesis of lipid A, a precursor of LPS, while the Lpt pathway is responsible for transporting fully assembled LPS molecules to the outer membrane. Novobiocin impacts the Lpt pathway by stimulating ATP hydrolysis[58], increasing LPS transport and disrupting membrane homeostasis[59]. Additionally, BCAL1364 and YhaI encode proteins containing the DUF805 domain and are predicted to be membrane-associated proteins. However, the precise function of DUF805 in bacterial membranes remains to be elucidated. These findings highlight the multifaceted nature of novobiocin's mode of action and uncover previously unknown determinants of novobiocin sensitivity.

We observed depletion (**Fig. 5A-B**) and clonal enhanced sensitivity (**Fig. 5D**) of knockdown mutants targeting *pth*, *rpsA*, *mnmA*, amino-peptidase p, and *waaA* when CIMPLE was exposed to PHAR(A). RpsA, MnmA, Pth, and aminopeptidase P are involved in the synthesis and regulation of proteins within the cell (**Fig. 6**). While MnmA, RpsA, and aminopeptidase P may not be directly targeted by PHAR(A), translation is a highly interconnected process and disruption of any of these components could have cascading effects on translation, tRNA modification, and peptide metabolism. RpsA serves as a gatekeeper at the ribosomal entrance, facilitating mRNA binding and initiation of translation[60]. Concurrently, MnmA modifies tRNAs, ensuring their fidelity in decoding mRNA codons, thus directly influencing the precision of protein synthesis[61]. Pth plays a crucial role in recycling peptidyl-tRNAs during translation termination, cleaving peptidyl-tRNAs to liberate completed polypeptides from the ribosome, thereby ensuring the generation of intact and functional proteins[56]. Complementing this process, aminopeptidase P degrades surplus peptides into amino acids, contributing to cellular recycling and maintaining metabolic equilibrium[62]. Inhibition of peptidyl-tRNA hydrolase (Pth) disrupts translation termination and peptide recycling, impairing protein synthesis. Reduced protein synthesis affects the availability of newly synthesized enzymes and proteins, including ribosomal proteins (*i.e.* RpsA and RplT), tRNA modification enzymes (*i.e.* MnmA), and peptide metabolism enzymes (*i.e.* aminopeptidase p). The dysregulation of translation, tRNA modification, and peptide metabolism induced by Pth inhibition can lead to cellular stress, altered metabolism, and cell death. *waaA* encodes a transferase involved in the biosynthesis of lipopolysaccharides (LPS) in gram-negative bacteria. WaaA catalyzes the addition of an acyl chain to the lipid A portion of LPS[63]. LPS is a major component of the outer membrane of gram-negative bacteria. This acylation modification is essential for the proper structure and function of LPS. It helps stabilize the outer membrane, contributes to its impermeability, and modulates the innate immune response during bacterial infections[64]. The absence of functional WaaA and the consequent truncation of LPS can enhance the permeability of the bacterial outer membrane, enhancing their susceptibility to antibiotics[63,65]. Additionally, alterations in LPS structure may compromise the integrity of the cell envelope, weakening the bacterial defense mechanisms against antibiotic-induced damage.

While CIMPLE provides a valuable tool for identifying potential drug-target interactions, we acknowledge the following limitations. Firstly, the 67 mutants present in CIMPLE at relatively high abundance may limit the detection of weak or indirect drug-target interactions specific to

those targets. We expect this to be minimized by optimizing the library by reiterating the relative abundance of mutants in the CIMPLE library. Secondly, the polar effect of CRISPRi, which represses transcription of downstream genes within the same operon, may complicate the interpretation of drug-target interactions, potentially obscuring the direct target(s)[6]. The putative drug(s) can be validated with follow-up experiments with our arrayed library, partially mitigating the problem. Finally, while PHAR(A) is a specific inhibitory of the Pth, it shows low target affinity. Structural characterization of Pth in complex with PHAR(A) will aid in the rational design of PHAR(A) analogs with greater affinity and stronger antibacterial activity.

Methods

Data Reporting

No statistical methods were used to predetermine sample size. The experiments were not randomized, and investigators were not blinded to allocation during experiments and outcome assessment.

Bacterial strains and growth conditions

Bacterial strains used in this study are provided in **Supplementary Table 8**. All strains were grown in LB-Lennox medium (Difco) at 37°C with continuous shaking at 230rpm unless otherwise specified. The following selective antibiotics were used: trimethoprim (Sigma; 50 µg/mL for *E. coli* strains and 100 µg/mL for *B. cenocepacia* strains). All plasmids used in this study are listed in **Supplementary Table 9**. L-rhamnose (Sigma) stock solution was prepared to 20% in de-ionized water and then filter sterilized.

Designing the sgRNAs

The sgRNAs were designed using a custom Python script that produces an output file containing ready-to-order primers to clone the sgRNAs. Briefly, the script splits the genome (in Genbank format) into two vectors (forward and reverse strand) and extract the sequence based on a provided query range. For example, if the script has a query range of -100 to +50 for a given

gene, the script will extract 150bp, 100bp upstream and 50bp downstream of the translation start site (ATG). The script will then look for the possible sgRNAs based on the availability of the PAM sites and extract the candidate sgRNAs. The candidate 20bp sgRNAs are then mapped to the genome to determine the specificity by paring one base at a time from the 3' end up to 12bp and will select the one sgRNA per gene that does not have off-target binding sites, free of homopolymer stretches (≥ 5) and closest to the ATG site. The script is customizable and can be modified to target the whole genome or only the essential genome, alter the query range, and provide more than one sgRNA per gene, if necessary. The provided sgRNAs are 20bp long and are then concatenated with the sgRNA scaffold sequence to predict the secondary structure folding of the hairpin required for dCas9 binding using Quikfold algorithm from the UNAFold package (http://unafold.rna.albany.edu/?q=DINAMelt/Quickfold). Successful sgRNAs are then concatenated with the pre-designed forward primer as a 5' extension and used for cloning the sgRNAs. The operon information to select the targets was collected from the DOOR database[35] and manually adjusted based on the transcriptomic data from Sass *et al.* [36]. The *B. cenocepacia* K56-2 genome sequence and the operon file were used as input for the Python script to design the sgRNAs. The sgRNA sequences are provided in **Supplementary Table 3**.

Cloning the sgRNAs and construction of the CRISPRi EGML

The CRISPRi mutants were created in an arrayed manner as previously described[32], with some modifications to create the mutants in a high-throughput fashion. Briefly, the selected sgRNAs were added as 5'-tail to a forward primer (sequence: 5'–GTTTTAGAGCTAGAAATAGCAAGTTAAAATAAGGC – 3') that binds to the promoter region of the sgRNA expressing plasmid (pgRNA). The resulting primers were ordered in 96-well format from IDT. All primers used in this study are listed in **Supplementary Table 10**. The sgRNA sequences were cloned into the pgRNA by inverse PCR using reverse primer 1092 and blunt-end ligated (30mins at 37ºC). PCR was performed using Q5 DNA polymerase with high-GC buffer using the following condition: 98ºC-5mins, 98ºC-30s, 30 cycles (98ºC-10s, 60ºC-30s, 72ºC-5mins), 72ºC-2mins, 12ºC-∞. The circularized plasmids were transformed into *E. coli* DH5α chemical competent cells. PCR amplification of the sgRNAs, cloning into pgRNA, and transformation into *E. coli* DH5α were performed in a 96-well format (**Supplementary Method**) in 96-well PCR plates (Sarstedt). The *E. coli* DH5α cells harbouring the sgRNA plasmids were

delivered into a *B. cenocepacia* K56-2 mutant expressing $dCas9_{Spy}$ (K56-2::*dCas9*$_{Spy}$) by conjugation.

Growth curves and clonal growth analysis of the CRISPRi EGML

The mutants were grown overnight into 96-well plates containing LB medium, selection antibiotic (trimethoprim 100µg/mL) and with/without 1% rhamnose (the $dCas9_{Spy}$ inducer) at 37ºC with continuous shaking (230 rpm). Overnight cultures were back diluted to OD_{600} of 0.01 and re-arrayed into 96-well plates in duplicate with and without 1% rhamnose. The mutants were grown at 37ºC with continuous shaking at 230 rpm. Mutant growth was measured at OD_{600} in real-time using a BioTek Synergy 2 microplate reader. One hundred and five mutants showed an observable growth defect when subcultured 4 h in the presence of rhamnose. The data from the microplate reader was processed in R (version 4.3.0). Clonal maximal growth rates (μ_{max}) and apparent lag times were calculated from the microplate growth curve data using 'growth rates' R package[66] applying 'easylinear' method. This approach involves fitting linear model segments to logarithmically transformed data to calculate the μ_{max}.

Creating equal and artificially depleted pools

To create the 'equal' and 'depleted' pools, the mutants were grown overnight in 96-well format at 37ºC with continuous shaking at 230 rpm. The overnight cultures were back diluted in 1:100, and the culture optical density was measured and pooled at final OD_{600} of 2.00. An equal volume of LB with LB plus 40% glycerol was added to the pool. The final pool was mixed well by pipetting. All the mutants were pooled at equal abundance in the 'equal pools,' and the appropriate mutants were added at lower abundances (0.5X to 100X) in the 'depleted pool .' Neat DMSO was added at final concentration of 20% (v/v) to the pools, treated at 95ºC for 5 mins in a thermocycler and stored in the -80ºC freezer.

Creating the optimized pooled EGML (CIMPLE pool), growth analysis and sensitizing rhamnose concentration determination

The essential gene knockdown mutants were pooled as described above to create "equal EGML ." All the mutants were pooled at equal abundances measured based on OD_{600}. The 'equal

EGML' was grown for 4h with and without rhamnose first (to mimic the clonal sub-culturing condition) or directly grown in different rhamnose concentrations ranging from 0 to 1% for 8h (~10–12 generations) in 96-well plates (Sarstedt) at 37ºC (**Supplementary Fig. 7**). Neat DMSO was added to the pools at 20% final concentration (v/v) and treated at 95ºC for 5 mins in a thermocycler and stored in the -80ºC freezer. The 5X3X2X, 10X5X3X and 20X10X5X pools were created similarly, except the inoculum of selected mutants was increased from 2X to 20X as indicated. Samples were prepared for CRISPRi-Seq as described below (see *NGS library preparation and CRISPRi-Seq*).

Multivariate polynomial regression modeling to predict the mutant depletion

Mutant depletion was estimated using a random forest regression model from 'sklearn.ensemble' package in Python. Depletion values were calculated based on a combination of multiple decision trees, each providing its own estimation. Clonal growth features (μ_{max} and apparent lag time in the presence of 1% rhamnose) were first transformed (feature engineered) into polynomial features using 'PolynomialFeatures' package in Python to capture potential non-linear relationships. A random forest regression model was fit to the transformed features and the pooled depletion data. The fitted model was applied to estimate the percent depletion values for the mutants based on the given input features.

NGS library preparation and CRISPRi-Seq

The mutant pools (equal pools, depleted pools and the optimized EGML) were used as templates for PCR to amplify the N_{20} sgRNA region. To avoid issues related to amplification errors, the number of PCR cycles was limited to a cycle that corresponds to ~25% maximum product. The number of cycles corresponding to ~25% maximum product was quantified by semi-quantitative PCR (**Supplementary Fig. 12**). Illumina flow cell adaptor, Nextera index, and sequencing primer binding site were added as 5' extension to the forward primer (sequence 5'-ACATTGACATTGTGAGCG-3') and reverse primer (sequence primer 5'-ACTTGCTATTTCTAGCTC-3') to enable 1-step PCR amplification. Resultant primers were used for PCR with Q5 DNA polymerase with high-GC buffer (NEB). For CRISPRi-Seq, 2 × 50µL PCR reactions were set up using the following amplification conditions: 98ºC-30s, 18 cycles (98ºC-10s, 52.4ºC-30s, 72ºC-20s), 72ºC-1mins, 4ºC- ∞. PCR products were cleaned with SeraMag beads

(Cytiva) and analyzed on a TapeStation4150 (Agilent Technologies). Amplicons were sequenced on an Illumina MiSeq (Jörg Stetefeld laboratory, University of Manitoba) for the equal and depleted pools with a MiSeq reagent kit v2 micro (PE 60 bp reads) and 20% PhiX spike.

Pilot screening of antibiotics with CRISPRi-Seq

B. cenocepacia K56-2 wild-type was exposed to a 2-fold gradient of different antibiotics in LB broth to determine the concentration that inhibits 30% of wild-type growth (IC_{30}; **Supplemental Table. 6**). The frozen optimized pooled EGML (OD_{600} 1.00) was thawed at room temperature and added to 4-mL LB broth in a 5' glass tube. The culture was incubated at 37°C with shaking at 230 rpm for 3 hours to recover the cells. The optimized pooled EGML was then exposed to the IC_{30} concentration of different antibiotics (or 1% DMSO control) for 8h (~10–12 generations) in 96-well plates (Sarstedt) in a humidity-controlled chamber at 37°C. 20% (final concentration v/v) DMSO was added to the wells after 8h and treated at 95°C for 5 mins in a thermocycler. The samples were prepared for CRISPRi-Seq as described above. Sequencing was performed on an Illumina MiSeq (Donnelly Centre, Toronto, Canada) with a MiSeq reagent kit v3 (PE 60bp reads), 20 dark cycles and 20% PhiX spike.

sgRNA counts from Illumina NGS to infer mutant fitness

sgRNAs were counted from the CRISPRi-Seq data using 2FAST2Q[67]. Since sequencing reads had a consistent structure, the locations of sgRNA sequences within each sequencing read in the demultiplexed FASTQ files (fastq.gz), along with the sgRNA sequence table, were provided as input. The output is a comma-separated value (CSV) file with one line per strain and well combination. The raw read counts were analyzed using DESEq2[68] package in R, as previously mentioned[69]. Mutant proportions were determined as the percent ratio between the reads corresponding to each mutant and the total reads within a sample. Relative abundance was calculated as the percent ratio between each mutant proportion after and before pooled growth. Percent depletion was calculated as 100- relative abundance.

Pth expression, purification and enzymatic activity analysis

Pth (BCAL0798) was expressed from a pET22b(+) vector under the control of an IPTG-inducible promoter. First, Pth was PCR amplified from wild-type *B. cenocepacia* K56-2 genome using Q5 polymerase with high GC buffer (NEB) and primers 3107 and 3108 (**Supplementary Table 10**) based on the following amplification condition: - 98ºC for 30s, 30 cycles (98ºC for 10s, 60.5ºC for 20s and 72ºC for 45s), 72ºC for 2mins and 4ºC- ∞. The 611bp amplicon and the pET22b(+) vector were double-digested with *NdeI* and *NotI*. Digested products were cleaned using Monarch® PCR & DNA Cleanup Kit (NEB) and incubated with T4 DNA ligase (NEB) overnight at 16ºC. The resulting plasmid, pPTH_BC_C2 was transformed into chemical-competent *E. coli* BL21(DE3) Gold cells, and ampicillin-resistant colonies were screened by colony PCR with primers 3008 and 3109.

For Pth purification, overnight cultures of *E. coli* cells harboring the plasmid were back diluted in 1:100 in LB (+100µg/mL ampicillin) and grown at 37ºC with shaking until the OD600nm of 0.6 was reached. After that, isopropyl β-D-1-thiogalactopyranoside (IPTG) was added to a final concentration of 1mM to induce the protein expression and the culture was incubated at 20ºC overnight. Cells were harvested via centrifugation, and the resulting cell pellets were resuspended in W/L buffer (50mM Tris-HCl pH 7.5, 500mM NaCl, 25mM imidazole) and stored at −80°C for at least 3 h. After thawing the pellet, 1mM phenylmethylsulfonyl fluoride (PMSF), 10mM $MgCl_2$, and DNaseI was added to the suspension and incubated at room temperature for 5 mins. EmulsiFlex-C3 (Avestin) was used to lyse the cells. After centrifugation, the 6x His-tagged Pth_{BC} was purified from the soluble lysate via a nickel-NTA gravity column, followed by washing with 250ml of W/L buffer and elution with elution buffer (50mM Tris-HCl at pH 7.5, 500mM NaCl, and 500mM imidazole). The samples were passed through SnakeSkin (Thermo Scientific) 10K MWCO dialysis membrane overnight at 4ºC for desalting and buffer exchange to remove imidazole.

Peptidyl-tRNA was synthesized and purified based on native chemical ligation (NCL) as described before[70]. All three compounds were resuspended to the desired concentration in 95:5 Ethanol: DMSO solution. 1nM Pth_{BC} was incubated in the reaction buffer (20mM HEPES-KOH, pH 7.2, 100mM NH_4Cl, CH_3COOK, 10mM $MgCl_2$, and 1mM DTT) with formyl-Met-Thr-His-Ser-Met-Arg-Cys-$tRNA^{Cys}$ (fMTHSMRC-$tRNA^{Cys}$) in the presence (or absence) of the compounds. The hydrolysis reaction was quenched by mixing the sample with acidic gel loading

buffer (Urea 7M, 100mM CH_3COONa pH 5.2, 0.05% bromophenol blue, 0.05% xylene cyanole, 0.25% SDS, 10mM EDTA, 10% β- Mercaptoethanol) in 1:2 ratio. Before loading samples, the polyacrylamide gel (16x10 cm; 7M Urea, 12% acrylamide: bisacrylamide 19:1, 100mM CH_3COONa pH 5.2) was pre-run in running buffer (100mM CH_3COONa pH 5.2, 1mM EDTA) for an hour at 80V. The sample slots in the gel were washed right before loading the samples to aid in even loading and remove urea from the slots. The samples were run in the running buffer at 120V in a cold room (4°C) for 16 hours and stained with ethidium bromide (EtBr) solution in a staining tray for 5-10 minutes with shaking. The sensitivity of EtBr in acidic conditions is lower; therefore, before staining, the gels were washed several times in 1X TBE (2 minutes each wash). After staining, the gel was washed in 1X TBE for 5-10 minutes to reduce the background. The gel was visualized using the ChemiDoc MP imaging system (BioRad).

Data representation

All graphs, except for the clustering images in **Fig. 3C-D**, were created and generated using R (version 4.3.0). For the clustering graphs, analyses were performed using 'sklearn.manifold' and 'sklearn.cluster' packages in Python in an anaconda environment. The plots were visualized with 'matplotlib.pyplot' in Python. All correlations were calculated using the Pearson method unless otherwise noted. Schematics were created with Biorender web tool (https://www.biorender.com/). The band intensity of the cleaved and uncleaved peptidyl-tRNA was measured using ImageJ. Chemical structures in **Supplementary Fig. 11** were created with ChemDraw. Panels in the figures are compiled with Affinity publisher 2.

Code and source data availability

All the raw read counts and source data for the figures and Python scripts (including the sgRNA design script) are available at https://github.com/zisanurrahman/CRISPRi_EGML_Main. The sequence of the closed K56-2 genome is under NCBI accession: NZ_LAUA00000000.1.

Acknowledgements

This work was supported by grants from the Canadian Institutes of Health Research (CIHR), Cystic Fibrosis Foundation, Cystic Fibrosis Canada to STC. ASMZR and JNN were

supported by a University of Manitoba Graduate Fellowship (UMGF). AD was supported by a Mitacs Globalink Research Award. The authors thank Dr. Andrew M. Hogan for the insightful scientific discussions and for critically reading the manuscript.

Competing interests

The authors declare no competing financial interests.

Figures

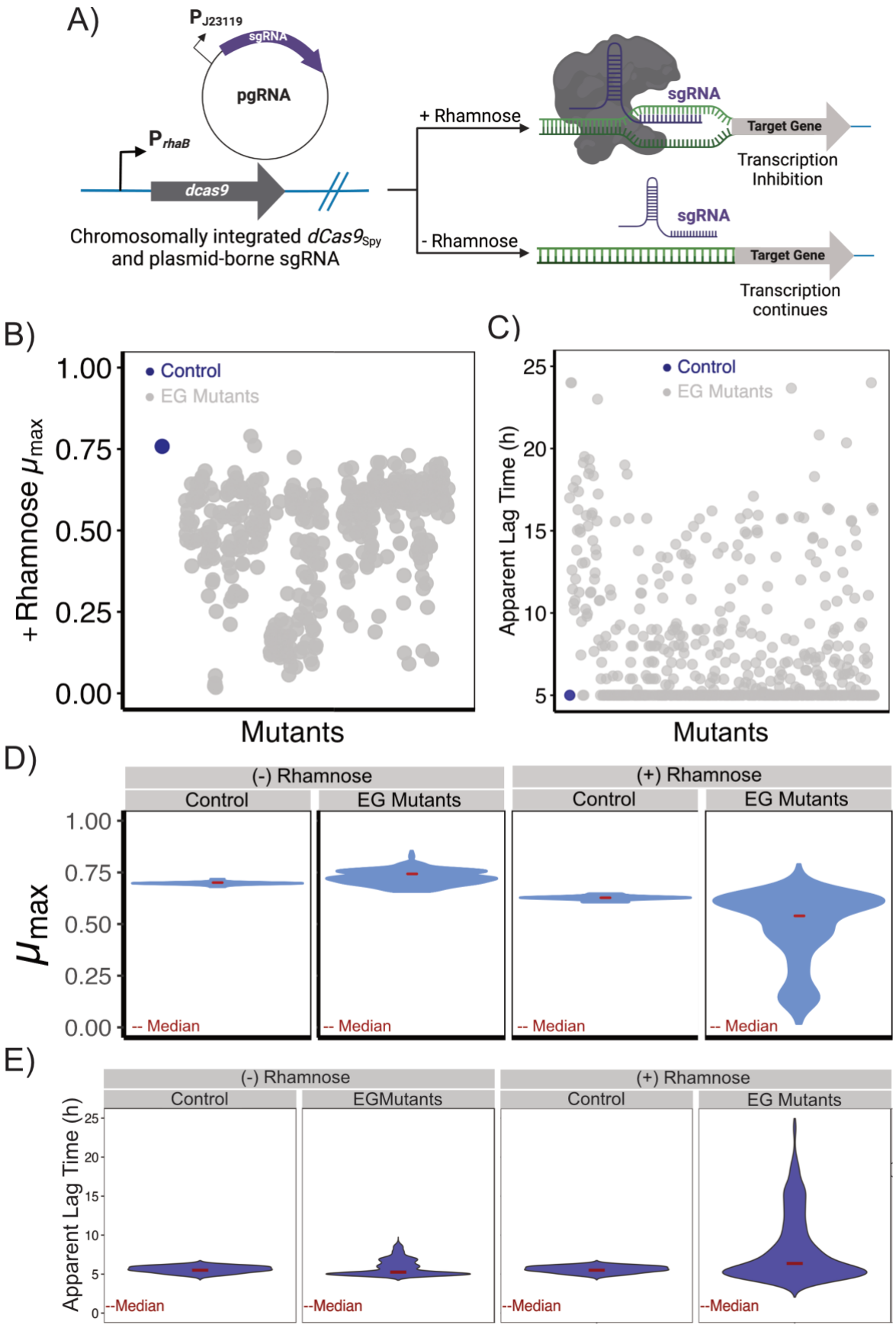
A)
P J23119
sgRNA
pgRNA
P rhaB
dcas9
Chromosomally integrated dCas9Spy
and plasmid-borne sgRNA
+ Rhamnose
sgRNA
Target Gene
Transcription
Inhibition
- Rhamnose
sgRNA
Target Gene
Transcription
continues
B)
Control
EG Mutants
+ Rhamnose μmax
1.00
0.75
0.50
0.25
0.00
Mutants
C)
Control
EG Mutants
Apparent Lag Time (h)
25
20
15
10
5
Mutants
D)
(-) Rhamnose
(+) Rhamnose
Control
EG Mutants
Control
EG Mutants
μmax
1.00
0.75
0.50
0.25
0.00
-- Median
-- Median
-- Median
-- Median
E)
(-) Rhamnose
(+) Rhamnose
Control
EGMutants
Control
EG Mutants
Apparent Lag Time (h)
25
20
15
10
5
0
--Median
--Median
--Median
--Median

Fig. 1: Construction and characterization of an arrayed essential gene mutant library (EGML) using CRISPRi. A) The EGML was constructed based on a $dCas9_{Spy}$ based CRISPRi system previously developed for *Burkholderia*. The system consists of a chromosomally integrated *dCas9* under a rhamnose-inducible promoter and plasmid-borne sgRNA. The image was reconstructed from Hogan et al. [32] and created with Biorender. B-E) Maximum growth rate (μ_{max}) (B and D) and apparent lag time (C and E) of the individual essential gene knockdown mutants and their distribution in the presence of rhamnose. The blue dot indicates the pgRNA-nontarget control, and the grey dots indicate individual essential gene mutants.

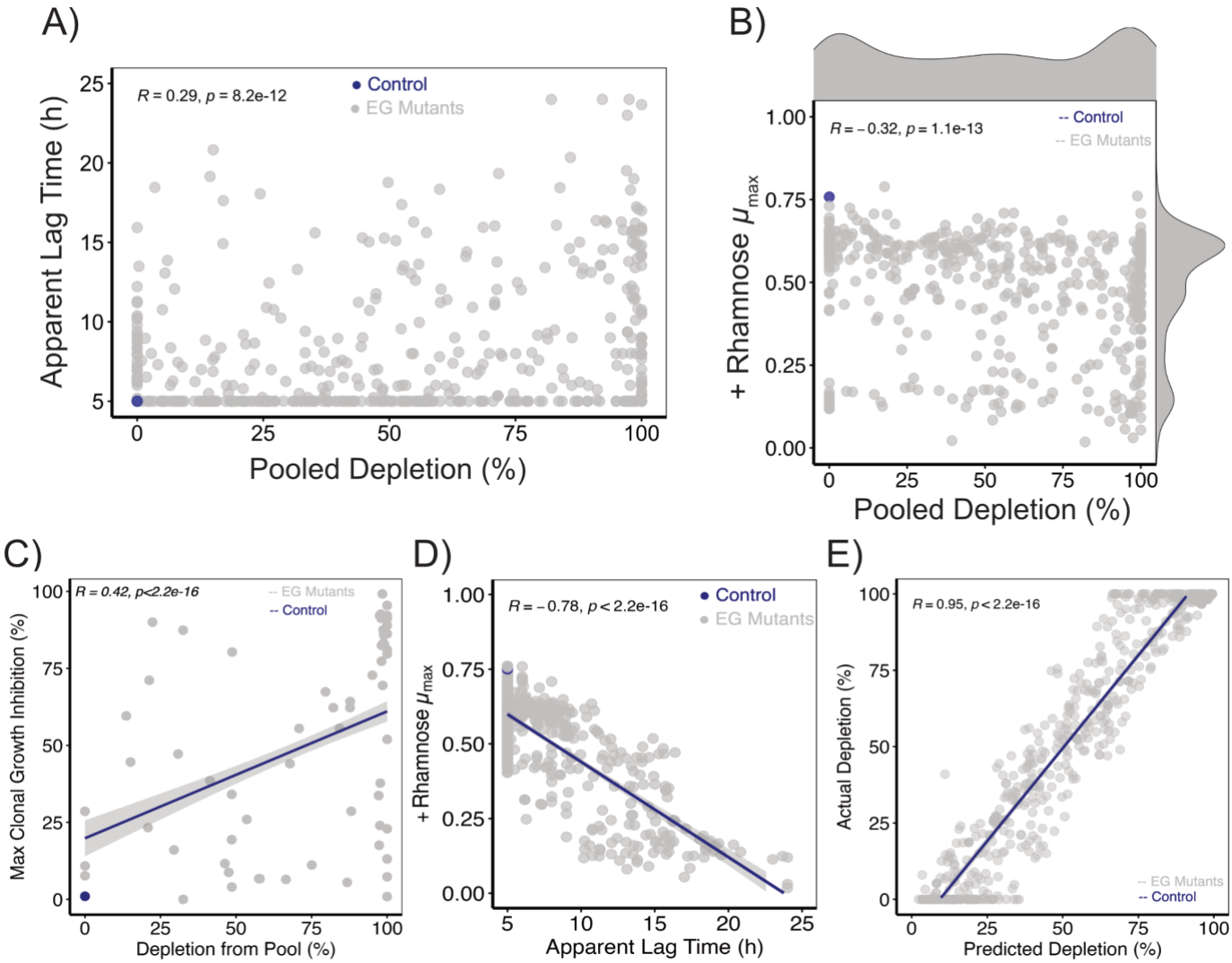

Fig. 2: EGML strain depletion during pooled growth is related to the clonal growth rate (μ_{max}) and apparent lag time. A-B) Correlation of clonal lag time (A) and μ_{max} (B) with the relative percent depletion of the mutant from the 1X (equal) pool. C) Comparison of the maximum percent clonal growth inhibition against the depletion from 1X pool during pooled growth of the mutants. Data shown for 40 EGML mutants. D) Correlation of clonal μ_{max} with apparent lag time of the EGML strains in the presence of rhamnose. E) Comparison of estimated and experimentally derived mutant depletion from the 1X pool. Estimated mutant depletion was calculated based on the clonal growth characteristics ($\mu_{max\ (+Rha)}$ and apparent lag time). The correlation coefficient was calculated based on the Pearson method. The mutant relative abundance (RA) in the pools was calculated based on the proportions of reads for the mutants in a pool and then compared to a control pool that had not been grown after pooling. Results are the mean of two independent

biological replicates. The blue dot indicates the non-targeting control, and each grey dot indicates an individual EGML mutant strain. Blue lines in panels C and D indicate the regression lines.

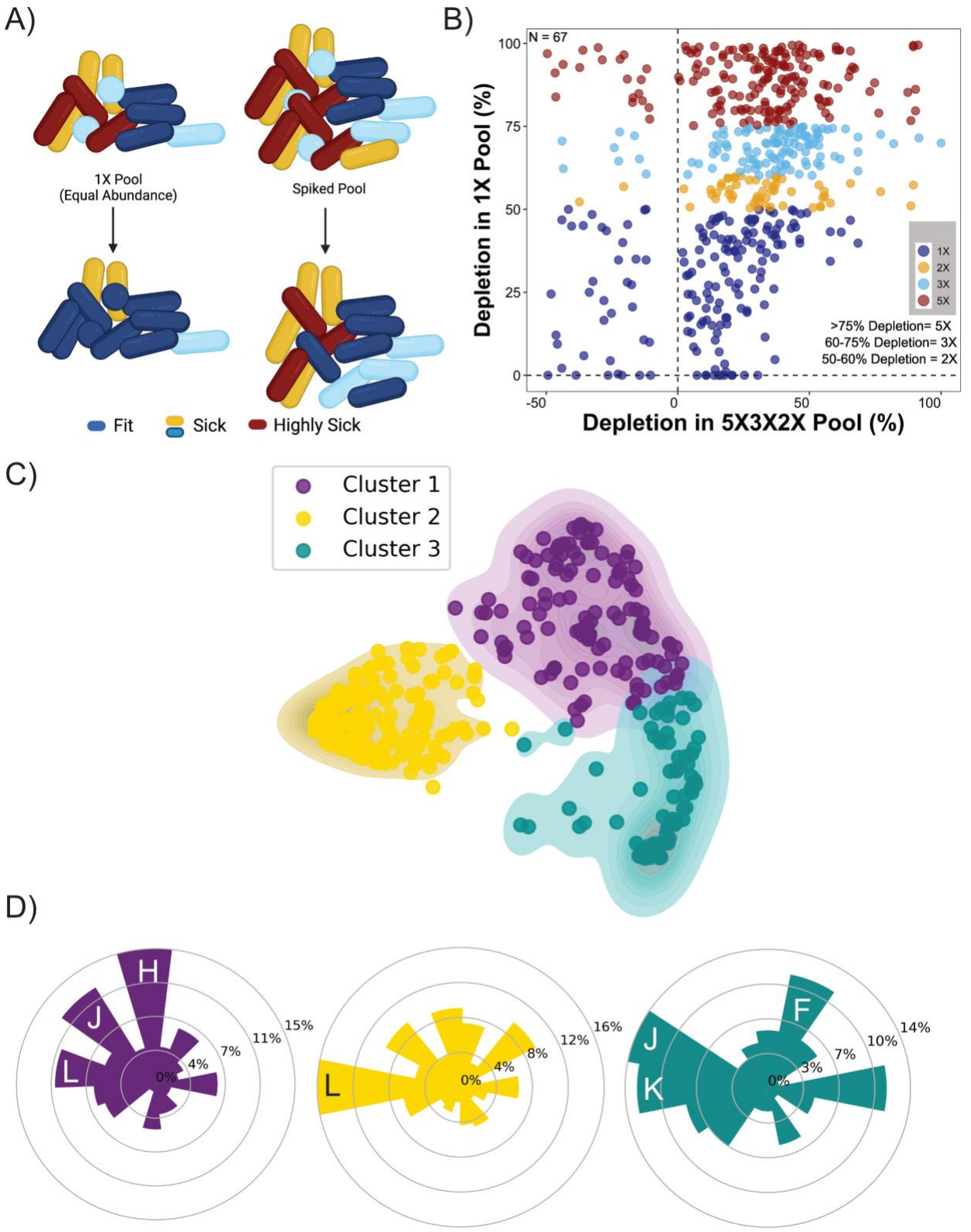

Fig. 3: Spiking of the sick EGML strains enables recovery of the mutants in the spiked pool. A) Schematic illustrating the relative fitness of the CRISPRi mutants in the 1X and spiked pool. Increasing the initial relative abundance of the highly sick mutants conferred a competitive advantage, enhancing their fitness. B) Comparison of mutant depletion between the 1X (equal) and 5X3X2X spiked pools. The mutant relative abundance (RA) in the pools was calculated based on the proportions of reads for the mutants in a pool and then compared to a control pool that had not been grown after pooling. Negative depletion indicates enrichment of the mutants compared to the control. Results are the mean of two independent biological replicates. C) Kernel PCA with K-means clustering of the mutants based on the clonal characteristics (μ_{max} and apparent lag time) and percent depletion from the pool. D) Percent of COGs in each cluster from panel C.

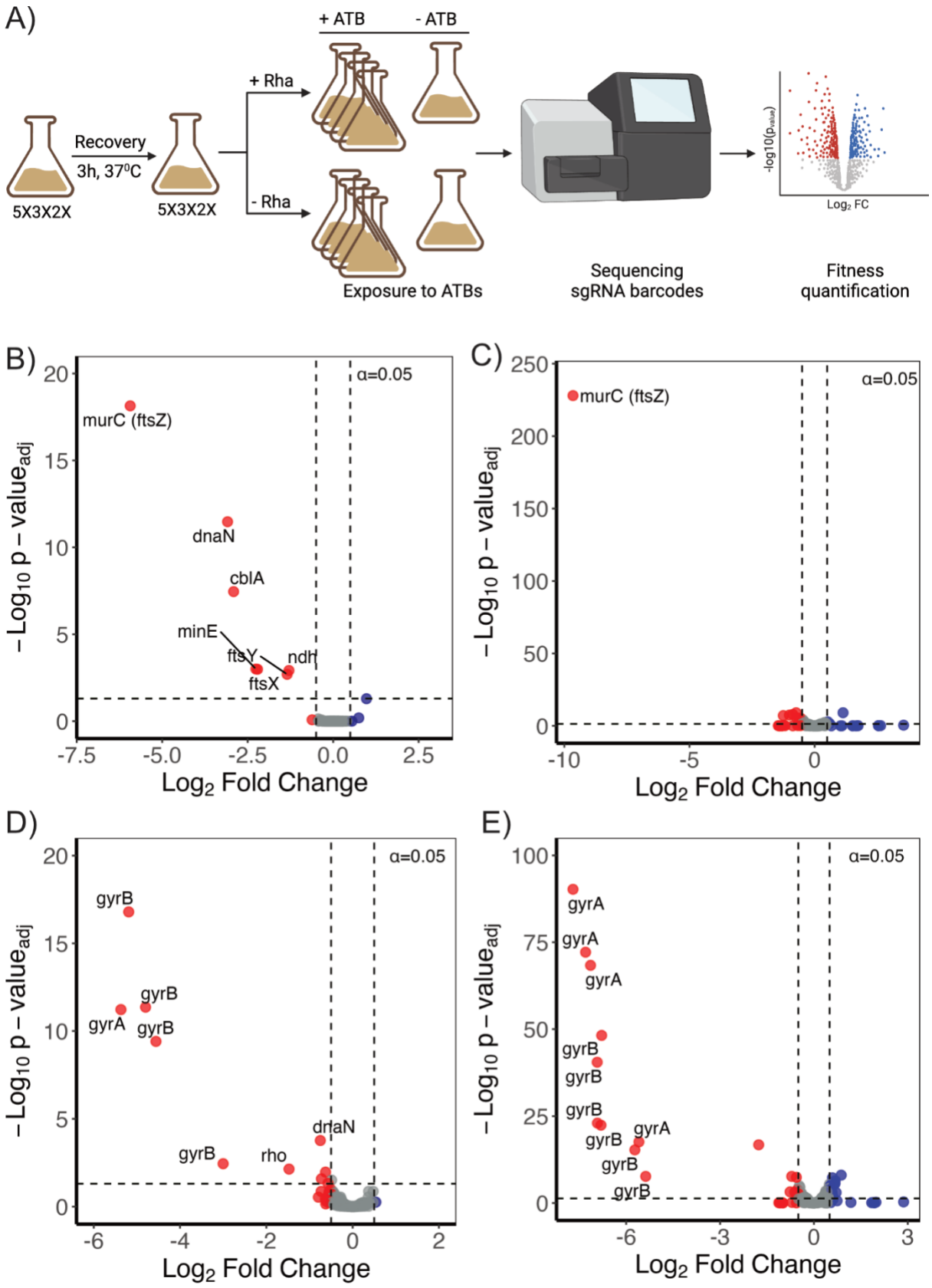
A)
+ ATB
- ATB
+ Rha
- Rha
Recovery
3h, 37°C
5X3X2X
5X3X2X
Exposure to ATBs
Sequencing
sgRNA barcodes
Fitness
quantification
Log2 FC
B)
α=0.05
murC (ftsZ)
dnaN
cblA
minE
ftsY
ftsX
ndh
– Log10 p – valueadj
Log2 Fold Change
C)
α=0.05
murC (ftsZ)
– Log10 p – valueadj
Log2 Fold Change
D)
α=0.05
gyrB
gyrA
gyrB
gyrB
dnaN
gyrB
rho
– Log10 p – valueadj
Log2 Fold Change
E)
α=0.05
gyrA
gyrA
gyrA
gyrB
gyrB
gyrB
gyrB
gyrA
gyrB
gyrB
– Log10 p – valueadj
Log2 Fold Change

Fig. 4: CRISPRi-Seq identifies known and novel drug-target interactions. A) Overview of the CRISPRi-Seq workflow. Exposure of the CIMPLE pool to subinhibitory concentration (IC_{30}) of C109 (B-C) and novobiocin (D-E). CIMPLE pool exposure to antibiotics without (B and D) and with (C and E) of 0.1% rhamnose. Blue and red dots represent enriched and depleted mutants (B-E), respectively. The horizontal dashed line indicates the significant threshold ($\alpha = 0.05$) (B-E). Vertical dashed lines indicate a $\log_2$ fold change of ±0.5. Results are the mean of two independent biological replicates.

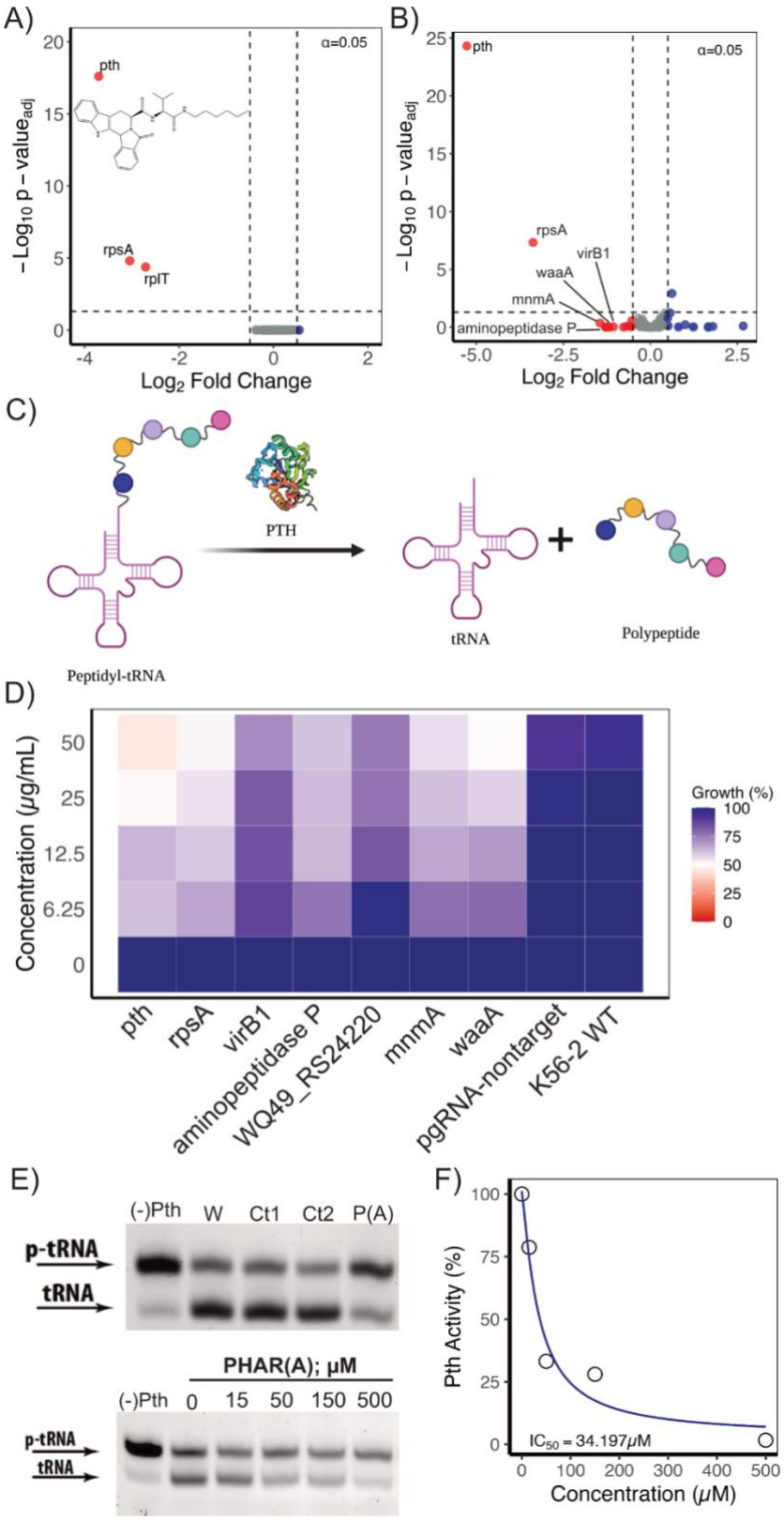

Fig. 5: PHAR(A) inhibits bacterial growth by impeding Pth activity. A-B) Exposure of the CIMPLE library to 50μM PHAR(A) without (A) and with (B) of 0.1% rhamnose. C) Schematic of the

Pth function. D) Exposure of a Pth CRISPRi mutant exhibited hypersensitivity to PHAR(A). E) *In vitro* inhibition of *B. cenocepacia* K56-2 Pth (Pth_{BC}) activity as shown by migration of intact peptidyl-tRNA (p-tRNA) and cleaved (t-RNA). F) Quantification of percent Pth activity based on the band intensity (in panel E) of the cleaved tRNA relative to the (-)Pth control. The band intensity was measured using ImageJ[72] and the IC_{50} was calculated using the "DRC"[73] package in R. Samples were electrophoretically separated in 12% polyacrylamide gel with 7M urea and stained with ethidium bromide. Water, Control compounds, and PHAR(A) are abbreviated as W, Ct and P(A), respectively, in panel E.

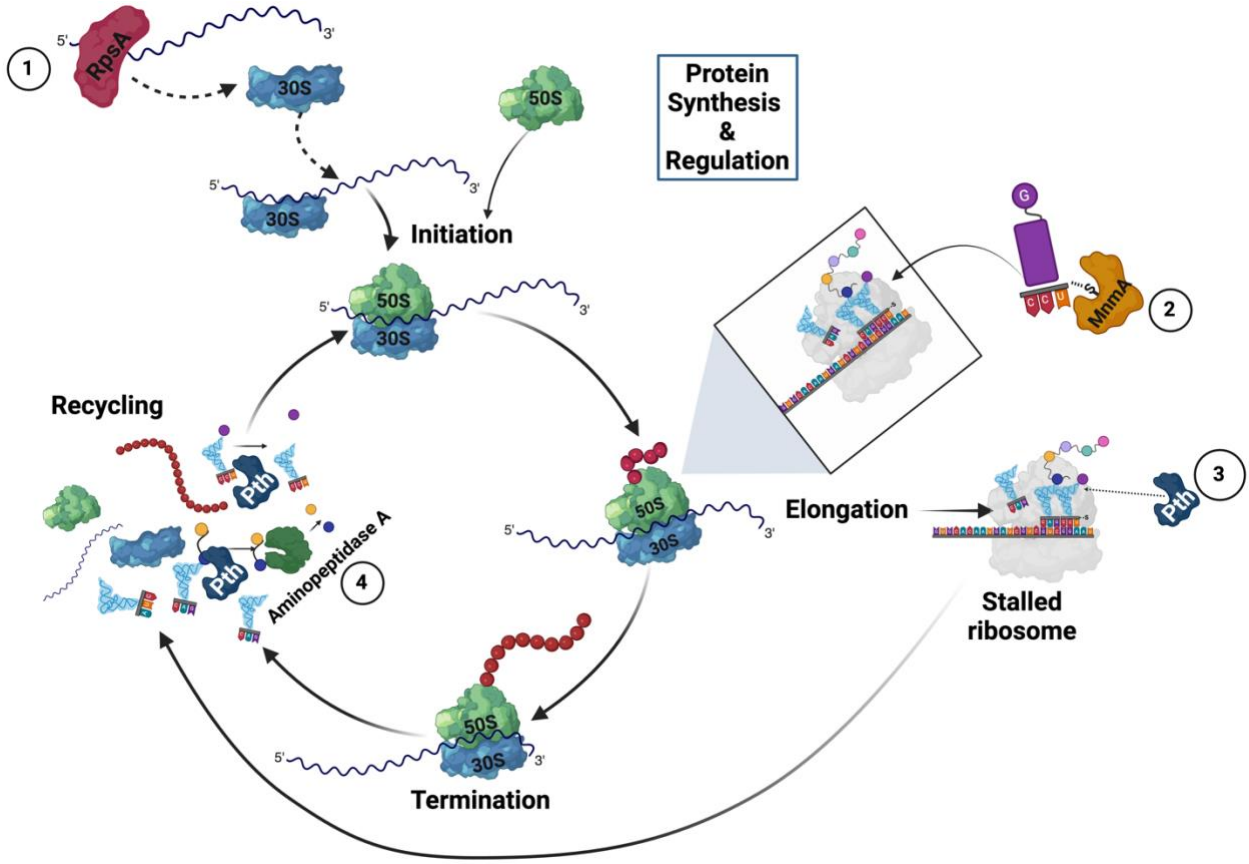

Fig. 6: Inhibition of peptidyl-tRNA hydrolase by PHAR(A) disrupts the overall translation process. RpsA (1), MnmA (2), Pth (3), and aminopeptidase A (4) are involved in different stages of protein synthesis and recycling.

References

1. Hogan, A. M. & Cardona, S. T. Gradients in gene essentiality reshape antibacterial research. *FEMS Microbiology Reviews* fuac005 (2022) doi:10.1093/femsre/fuac005.
2. Forsyth, R. A. *et al.* A genome-wide strategy for the identification of essential genes in Staphylococcus aureus. *Molecular Microbiology* **43**, 1387–1400 (2002).
3. Johnson, E. O. *et al.* Large-scale chemical–genetics yields new *M. tuberculosis* inhibitor classes. *Nature* **571**, 72–78 (2019).
4. Roemer, T. & Boone, C. Systems-level antimicrobial drug and drug synergy discovery. *Nat.Chem.Biol.* **9**, 222–231 (2013).
5. Cardona, S. T., Selin, C. & Gislason, A. S. Genomic tools to profile antibiotic mode of action. *Critical reviews in microbiology* **4**, 465–472 (2015).
6. Qi, L. S. *et al.* Repurposing CRISPR as an RNA-guided platform for sequence-specific control of gene expression. *Cell* **152**, 1173–1183 (2013).
7. Peters, J. M. *et al.* A comprehensive, CRISPR-based functional analysis of essential genes in bacteria. *Cell* **165**, 1493–1506 (2016).
8. Anders, C., Niewoehner, O., Duerst, A. & Jinek, M. Structural basis of PAM-dependent target DNA recognition by the Cas9 endonuclease. *Nature* **513**, 569–573 (2014).
9. Jinek, M. *et al.* Structures of Cas9 Endonucleases Reveal RNA-Mediated Conformational Activation. *Science* **343**, 1247997–1247997 (2014).
10. Sternberg, S. H., Redding, S., Jinek, M., Greene, E. C. & Doudna, J. A. DNA interrogation by the CRISPR RNA-guided endonuclease Cas9. *Nature* **507**, 62–67 (2014).
11. Gilbert, L. A. *et al.* Genome-Scale CRISPR-Mediated Control of Gene Repression and Activation. *Cell* **159**, 647–661 (2014).

12. Liu, X. *et al.* High-throughput CRISPRi phenotyping identifies new essential genes in *Streptococcus pneumoniae*. *Mol. Syst. Biol.* **13**, 931 (2017).

13. Rousset, F. *et al.* Genome-wide CRISPR-dCas9 screens in *E. coli* identify essential genes and phage host factors. *PLOS Genetics* **14**, e1007749 (2018).

14. Rishi, H. S. *et al. Systematic Genome-Wide Querying of Coding and Non-Coding Functional Elements in* E. Coli *Using CRISPRi*. http://biorxiv.org/lookup/doi/10.1101/2020.03.04.975888 (2020) doi:10.1101/2020.03.04.975888.

15. Wang, T. *et al.* Pooled CRISPR interference screening enables genome-scale functional genomics study in bacteria with superior performance. *Nat Commun* **9**, 2475 (2018).

16. Yao, L. *et al.* Pooled CRISPRi screening of the cyanobacterium Synechocystis sp PCC 6803 for enhanced industrial phenotypes. *Nat Commun* **11**, 1666 (2020).

17. Cui, L. *et al.* A CRISPRi screen in *E. coli* reveals sequence-specific toxicity of dCas9. *Nat Commun* **9**, 1912 (2018).

18. Jiang, W., Oikonomou, P. & Tavazoie, S. Comprehensive genome-wide perturbations via CRISPR adaptation reveal complex genetics of antibiotic sensitivity. *Cell* **180**, 1002-1017.e31 (2020).

19. Lee, H. H. *et al.* Functional genomics of the rapidly replicating bacterium *Vibrio natriegens* by CRISPRi. *Nat Microbiol* (2019) doi:10.1038/s41564-019-0423-8.

20. de Wet, T. J., Winkler, K. R., Mhlanga, M., Mizrahi, V. & Warner, D. F. Arrayed CRISPRi and quantitative imaging describe the morphotypic landscape of essential mycobacterial genes. *eLife* **9**, e60083 (2020).

21. St. Pierre, J., Roberts, J., Alam, M. A. & Shields, R. C. Construction of an arrayed CRISPRi library as a resource for essential gene function studies in *Streptococcus mutans*. *Microbiol Spectr* **12**, e03149-23 (2024).

22. Shields, R. C. *et al.* Repurposing the *Streptococcus mutans* CRISPR-Cas9 system to understand essential gene function. *PLOS Pathogens* **16**, e1008344 (2020).

23. Hawkins, J. S. *et al.* Mismatch-CRISPRi reveals the co-varying expression-fitness relationships of essential genes in *Escherichia coli* and *Bacillus subtilis*. *Cell Syst* **11**, 523-535.e9 (2020).

24. de Wet, T. J., Gobe, I., Mhlanga, M. M. & Warner, D. F. CRISPRi-Seq for the Identification and Characterisation of Essential Mycobacterial Genes and Transcriptional Units. *bioRxiv* 358275 (2018) doi:10.1101/358275.

25. McNeil, M. B., Keighley, L. M., Cook, J. R., Cheung, C.-Y. & Cook, G. M. CRISPR interference identifies vulnerable cellular pathways with bactericidal phenotypes in *Mycobacterium tuberculosis*. *Molecular Microbiology* **n/a**, (2021).

26. Li, S. *et al.* CRISPRi chemical genetics and comparative genomics identify genes mediating drug potency in Mycobacterium tuberculosis. *Nat Microbiol* **7**, 766–779 (2022).

27. Liu, X. *et al. Genome-Wide CRISPRi Screens Reveal the Essentialome and Determinants for Susceptibility to Dalbavancin in* Staphylococcus Aureus. http://biorxiv.org/lookup/doi/10.1101/2023.08.30.555613 (2023) doi:10.1101/2023.08.30.555613.

28. Ward, R. D. *et al. Essential Gene Phenotypes Reveal Antibiotic Mechanisms and Synergies in* Acinetobacter Baumannii. http://biorxiv.org/lookup/doi/10.1101/2022.11.09.515830 (2022) doi:10.1101/2022.11.09.515830.

29. Bosch, B. *et al.* Genome-wide gene expression tuning reveals diverse vulnerabilities of *M. tuberculosis*. *Cell* **184**, 4579-4592.e24 (2021).

30. Martin, J. K. *et al.* A dual-mechanism antibiotic kills Gram-negative bacteria and avoids drug resistance. *Cell* **181**, 1518-1532.e14 (2020).

31. Vial, L., Chapalain, A., Groleau, M. C. & Deziel, E. The various lifestyles of the *Burkholderia cepacia* complex species: a tribute to adaptation. *Environmental microbiology* **13**, 1–12 (2011).

32. Hogan, A. M., Rahman, A. S. M. Z., Lightly, T. J. & Cardona, S. T. A broad-host-range CRISPRi toolkit for silencing gene expression in *Burkholderia*. *ACS Synth. Biol.* **8**, 2372–2384 (2019).

33. Gislason, A. S., Turner, K., Domaratzki, M. & Cardona, S. T. Comparative analysis of the *Burkholderia cenocepacia* K56-2 essential genome reveals cell envelope functions that are uniquely required for survival in species of the genus *Burkholderia*. *Microb Genom* **3**, e000140 (2017).

34. Rahman, A. S. M. Z., Timmerman, L., Gallardo, F. & Cardona, S. T. Identification of putative essential protein domains from high-density transposon insertion sequencing. *Sci Rep* **12**, 962 (2022).

35. Mao, X. *et al.* DOOR 2.0: presenting operons and their functions through dynamic and integrated views. *Nucleic acids research* **42**, D654-9 (2014).

36. Sass, A. M. *et al.* Genome-wide transcription start site profiling in biofilm-grown *Burkholderia cenocepacia* J2315. *BMC Genomics* **16**, 775 (2015).

37. Larson, M. H. *et al.* CRISPR interference (CRISPRi) for sequence-specific control of gene expression. *Nat.Protoc.* **8**, 2180–2196 (2013).

38. Bikard, D. *et al.* Programmable repression and activation of bacterial gene expression using an engineered CRISPR-Cas system. *Nucleic Acids Research* **41**, 7429–7437 (2013).

39. Blin, K., Pedersen, L. E., Weber, T. & Lee, S. Y. CRISPy-web: An online resource to design sgRNAs for CRISPR applications. *Synthetic and Systems Biotechnology* **1**, 118–121 (2016).

40. Heigwer, F., Kerr, G. & Boutros, M. E-CRISP: fast CRISPR target site identification. *Nature methods* **11**, 122–123 (2014).

41. Heigwer, F. *et al.* CRISPR library designer (CLD): software for multispecies design of single guide RNA libraries. *Genome Biol* **17**, 55 (2016).

42. Liu, H. *et al.* CRISPR-ERA: a comprehensive design tool for CRISPR-mediated gene editing, repression and activation: Fig. 1. *Bioinformatics* **31**, 3676–3678 (2015).

43. Ma, M., Ye, A. Y., Zheng, W. & Kong, L. A Guide RNA Sequence Design Platform for the CRISPR/Cas9 System for Model Organism Genomes. *BioMed Research International* **2013**, 1–4 (2013).

44. Montague, T. G., Cruz, J. M., Gagnon, J. A., Church, G. M. & Valen, E. CHOPCHOP: a CRISPR/Cas9 and TALEN web tool for genome editing. *Nucleic Acids Research* **42**, W401–W407 (2014).

45. Wang, D. *et al.* Optimized CRISPR guide RNA design for two high-fidelity Cas9 variants by deep learning. *Nat Commun* **10**, 4284 (2019).

46. Xie, S., Shen, B., Zhang, C., Huang, X. & Zhang, Y. sgRNAcas9: A Software Package for Designing CRISPR sgRNA and Evaluating Potential Off-Target Cleavage Sites. *PLoS ONE* **9**, e100448 (2014).

47. Gislason, A. S. *et al.* Competitive growth enhances conditional growth mutant sensitivity to antibiotics and exposes a two-component system as an emerging antibacterial target in *Burkholderia cenocepacia*. *Antimicrob. Agents Chemother.* **61**, e00790-16 (2017).

48. Hogan, A. M. *et al.* Competitive fitness of essential gene knockdowns reveals a broad-spectrum antibacterial inhibitor of the cell division protein FtsZ. *Antimicrob Agents Chemother* **62**, e01231-18 (2018).

49. Mika, S. *et al.* Kernel PCA and De-Noising in Feature Spaces. in *Advances in Neural Information Processing Systems* (eds. Kearns, M., Solla, S. & Cohn, D.) vol. 11 (MIT Press, 1998).

50. Li, Y. & Wu, H. A Clustering Method Based on K-Means Algorithm. *Physics Procedia* **25**, 1104–1109 (2012).

51. Lutkenhaus, J. & Du, S. *E. coli* cell cycle machinery. *Subcell. Biochem.* **84**, 27–65 (2017).

52. Gellert, M., O'Dea, M. H., Itoh, T. & Tomizawa, J. Novobiocin and coumermycin inhibit DNA supercoiling catalyzed by DNA gyrase. *Proc.Natl.Acad.Sci.U.S.A.* **73**, 4474–4478 (1976).

53. Romano, K. P. & Hung, D. T. Targeting LPS biosynthesis and transport in gram-negative bacteria in the era of multi-drug resistance. *Biochim Biophys Acta Mol Cell Res* **1870**, 119407 (2023).

54. Rahman, A. S. M. Z. *et al.* A machine learning model trained on a high-throughput antibacterial screen increases the hit rate of drug discovery. *PLoS Comput Biol* **18**, e1010613 (2022).

55. Sharma, S. *et al.* Structural and functional insights into peptidyl-tRNA hydrolase. *Biochimica et Biophysica Acta (BBA) - Proteins and Proteomics* **1844**, 1279–1288 (2014).

56. Das, G. & Varshney, U. Peptidyl-tRNA hydrolase and its critical role in protein biosynthesis. *Microbiology* **152**, 2191–2195 (2006).

57. Zhao, H. *et al.* Depletion of Undecaprenyl Pyrophosphate Phosphatases Disrupts Cell Envelope Biogenesis in Bacillus subtilis. *J. Bacteriol.* **198**, 2925–2935 (2016).

58. May, J. M. *et al.* The Antibiotic Novobiocin Binds and Activates the ATPase That Powers Lipopolysaccharide Transport. *J Am Chem Soc* **139**, 17221–17224 (2017).

59. Okuda, S., Sherman, D. J., Silhavy, T. J., Ruiz, N. & Kahne, D. Lipopolysaccharide transport and assembly at the outer membrane: the PEZ model. *Nat Rev Microbiol* **14**, 337–345 (2016).

60. Delvillani, F., Papiani, G., Dehò, G. & Briani, F. S1 ribosomal protein and the interplay between translation and mRNA decay. *Nucleic Acids Res* **39**, 7702–7715 (2011).

61. Moukadiri, I. *et al.* Evolutionarily conserved proteins MnmE and GidA catalyze the formation of two methyluridine derivatives at tRNA wobble positions. *Nucleic Acids Research* **37**, 7177–7193 (2009).

62. Polacek, N. & Mankin, A. S. The Ribosomal Peptidyl Transferase Center: Structure, Function, Evolution, Inhibition. *Critical Reviews in Biochemistry and Molecular Biology* **40**, 285–311 (2005).

63. Nikaido, H. Molecular Basis of Bacterial Outer Membrane Permeability Revisited. *Microbiol. Mol. Biol. Rev.* **67**, 593–656 (2003).

64. Raetz, C. R. H. & Whitfield, C. Lipopolysaccharide endotoxins. *Annu Rev Biochem* **71**, 635–700 (2002).

65. Egan, A. J. F. Bacterial outer membrane constriction. *Molecular Microbiology* **107**, 676–687 (2018).

66. Petzoldt, T. growthrates: Estimate Growth Rates from Experimental Data.

67. Bravo, A. M., Typas, A. & Veening, J.-W. 2FAST2Q: a general-purpose sequence search and counting program for FASTQ files. *PeerJ* **10**, e14041 (2022).

68. Love, M. I., Huber, W. & Anders, S. Moderated estimation of fold change and dispersion for RNA-seq data with DESeq2. *Genome Biol* **15**, 550 (2014).

69. de Bakker, V., Liu, X., Bravo, A. M. & Veening, J.-W. CRISPRi-seq for genome-wide fitness quantification in bacteria. *Nat Protoc* **17**, 252–281 (2022).

70. Syroegin, E. A., Aleksandrova, E. V. & Polikanov, Y. S. Insights into the ribosome function from the structures of non-arrested ribosome–nascent chain complexes. *Nat. Chem.* **15**, 143–153 (2023).

71. Hoberecht, L., Perampalam, P., Lun, A. & Fortin, J.-P. A comprehensive Bioconductor ecosystem for the design of CRISPR guide RNAs across nucleases and technologies. *Nat Commun* **13**, 6568 (2022).

72. Schneider, C. A., Rasband, W. S. & Eliceiri, K. W. NIH Image to ImageJ: 25 years of image analysis. *Nat Methods* **9**, 671–675 (2012).

73. Ritz, C., Baty, F., Streibig, J. C. & Gerhard, D. Dose-Response Analysis Using R. *PLoS ONE* **10**, e0146021 (2015).